Currents and Conduction Losses in Unilateral Finline

CHRIS OLLEY AND T. ROZZI, SENIOR MEMBER, IEEE

Abstract—This paper presents a rigorous calculation of currents, conduction losses, and Q factors of the fundamental and higher order modes of unilateral finline. The latter, in particular, are important in estimating the loss for practical components. The approach is based on a Ritz–Galerkin variational development of, first, the field in the fin gap in terms of functions which intrinsically satisfy the edge condition and, second, the currents in the fin also satisfying the same properties.

Results show losses to be higher than previously estimated, in very good agreement with experiment.

I. Introduction

MUCH EFFORT currently is being directed at analyses of E-plane guiding structures. One of the earliest such structures to emerge was finline [1], a form of planar ridge waveguide. As the mathematical approaches evolved, notably the spectral-domain technique [2], analyses began to appear [3]. Results on dispersion, higher order modes [4], finite metallization thickness [5], etc., have been published by various workers. However, very little work was produced on the analysis of finline loss, with the exception of that by Davies [6] for the fundamental mode.

Higher order modes, however, are responsible for power storage at discontinuities occurring in practical components. Moreover, loss performance is one of the major drawbacks of finline. There is a need, therefore, for more detailed work, including an investigation of the wall currents and losses in higher order modes.

The analysis given here employs an expansion in the fin gap based upon the Schwinger functions as detailed in an earlier contribution [7], which includes a proper description of the edge condition. The inclusion of this effect is found to give higher losses than predicted by [6], in agreement with an experimental verification.

In addition, an alternative formulation of the obstacle type employing an expansion of the fin currents in appropriate Gegenbauer polynomials is presented here. In fact since information about the fin currents is obtained as a by-product of the loss analysis, it is interesting to observe the direct correspondence between these current distributions and those of the gap field. It was expected *a priori* that an aperture formulation as in [7] would be more appropriate for narrow fin gaps, whereas an obstacle formulation would be more effective for wide gaps. On the basis of the results, however, it is concluded that finline is best solved in terms of just an aperture formulation, within the range of gap apertures commonly used in practice.

Manuscript received February 17, 1987; revised July 23, 1987. This work was supported in part by the Sciences and Engineering Research Council under Grant GR/C/84170 and CASE Award 62375

C. Olley is with GEC-Marconi Research, Great Baddow, Essex, England

T. Rozzi is with the School of Electrical Engineering, University of Bath, Claverton Down, Bath BA2 7AY, England.

IEEE Log Number 8717904.

II. Analysis: Aperture Formulation

Consider the idealized unilateral finline structure given in Fig. 1. Since the dielectrically loaded waveguide formed by the substrate and housing supports only TE-to-y and TM-to-y modes, respectively, it is convenient to describe the fields in finline in terms of y-directed electric and magnetic Hertzian vector potentials so that

$$\boldsymbol{E} = -j\omega\mu\nabla\times\Pi_h + k^2\Pi_e + \nabla\nabla\cdot\Pi_e \tag{1}$$

$$\boldsymbol{H} = k^2\Pi_h + \nabla\nabla\cdot\Pi_h + j\omega\epsilon\nabla\times\Pi_e \tag{2}$$

where

$$\Pi_e = \Psi_h(x,y)e^{-j\beta z} \qquad \Pi_h = \Psi_e(x,y)e^{-j\beta z}.$$

These potentials are constructed from the eigenmodes of the structure without fins, and then coupled together to satisfy the boundary conditions given by the fin. These boundary conditions must include not only the normal metallic wall conditions but also the conditions given by the fin edge which makes finline modes hybrid.

Thus

$$\Psi_h(x,y) = \sum_n^{\infty} U_{hn}\phi_{hn}(x)\psi_{hn}(y) \tag{3}$$

$$\Psi_e(x,y) = \sum_n^{\infty} U_{en}\phi_{en}(x)\psi_{en}(y) \tag{4}$$

with

$$\phi_{hn}(x) = \sqrt{\frac{\delta_n}{a}}\cos\frac{n\pi}{a}x \qquad \phi_{en}(x) = \sqrt{\frac{2}{a}}\sin\frac{n\pi}{a}x$$

$$\delta_n = 2n > 0 \qquad \delta_0 = 1.$$

for symmetric modes. The above lead to field expansions of the form

$$E_x(x,y) = \sum_{n=0}^{\infty} E_{xn}\phi_{hn}(x)\chi_n(y) \tag{5}$$

where $\psi_n(y)$ are somewhat tedious to derive and can be found by substituting the potentials (3) and (4) into (1)

0018-9480/88/0100-0086$01.00

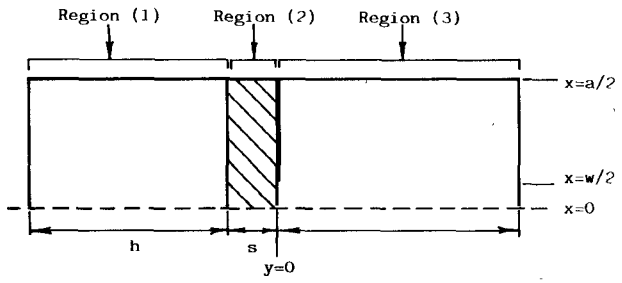

Fig. 1. Idealized unilateral finline—axis positioning and dimension details.

and (2). Expansions similar to (5) are thus found for the remaining components, as listed in Appendix I.

Using the concept of an equivalent transverse circuit, we readily formulate a system of integral equations describing the coupling effects of the fin. For fields to the right of $y = 0$,

$$\begin{bmatrix} -H_z(x) \\ \frac{\pi}{a}\int H_x(x)\,dx \end{bmatrix} = \int_{\text{fin gap}} \begin{bmatrix} Y_{11}^{R}(x,x') & Y_{12}^{R}(x,x') \\ Y_{21}^{R}(x,x') & Y_{22}^{R}(x,x') \end{bmatrix} \begin{bmatrix} E_x(x') \\ \frac{a}{\pi}\frac{\partial}{\partial x}E_z(x') \end{bmatrix} dx' \quad (6)$$

and for fields to the left

$$\begin{bmatrix} H_z(x) \\ -\frac{\pi}{a}\int H_x(x)\,dx \end{bmatrix} = \int_{\text{fin gap}} \begin{bmatrix} Y_{11}^{L}(x,x') & Y_{12}^{L}(x,x') \\ Y_{21}^{L}(x,x') & Y_{22}^{L}(x,x') \end{bmatrix} \begin{bmatrix} E_x(x') \\ \frac{a}{\pi}\frac{\partial}{\partial x}E_z(x') \end{bmatrix} dx' \quad (7)$$

where $Y^{L,R}$ are the Green's admittances of the cross section [7].

Solution for a finline mode is then obtained by imposing continuity of fields over the fin gap (which in fact corresponds to resonance of the transverse equivalent network, see Fig. 2). Hence by adding (6) and (7), we obtain the combined integral equations

$$\begin{bmatrix} \tilde{Y}_{11} & \tilde{Y}_{12} \\ \tilde{Y}_{21} & \tilde{Y}_{22} \end{bmatrix} \cdot \begin{bmatrix} E_x \\ \frac{a}{\pi}\frac{\partial}{\partial x}E_z \end{bmatrix} = 0 \quad (8)$$

where $\tilde{Y}_{ij}$ denotes the integral operator whose kernel is $Y_{ij}(x, x')$ of (6) and (7).

In order to achieve a solution of the integral equations for resonance while adequately representing the boundary conditions of the fin, we expand onto the basis space originally introduced by Schwinger for the analysis of infinitely thin irises [8] which implicitly satisfy the boundary conditions at the fin edges. With the above expansion, the integral equations are transformed into

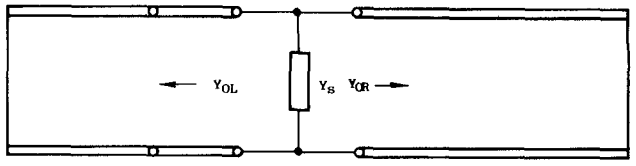

Fig. 2. Simplified transverse equivalent circuit.

matrix equations:

$$\begin{bmatrix} \boldsymbol{Y}_{11} & \boldsymbol{Y}_{12} \\ \boldsymbol{Y}_{21} & \boldsymbol{Y}_{22} \end{bmatrix} \begin{bmatrix} \boldsymbol{X} \\ \boldsymbol{Z} \end{bmatrix} = 0 \quad (9)$$

where the matrices are repeated in Appendix II for the sake of completeness.

As the Schwinger functions themselves have been derived from the conformal mapping of fields in a parallel-plate waveguide onto a waveguide with iris, convergence of the expansion is very fast. In fact for quasi-static cases, e.g. at cutoff, only one function is required. Recourse to matrix equations is only needed to allow for small dynamic corrections in the general solution, (2×2) matrices being all that is normally required. The Schwinger functions thus lead to a highly convergent solution for all finline modes.

Having obtained solution equation (9), the electric and magnetic fields within the finline can be determined from the field expansions, such as (5). The coefficients U_{en} and U_{hn} used to construct the potentials and, implicit in the functions $\psi_h(x, y)$ are obtained from the aperture field expansion as

$$U_{hn}^{R} = \frac{1}{j\omega\mu} \frac{-j\beta E_{xn} + \left[\frac{n\pi}{a}\right] E_{zn}}{\sqrt{\left[\frac{n\pi}{a}\right]^2 + \beta^2}} \quad (10)$$

$$U_{en}^{R} = \frac{Y_{nR}^{TM}}{j\omega\epsilon} \frac{\left[\frac{n\pi}{a}\right] E_{xn} - j\beta E_{zn}}{\sqrt{\left[\frac{n\pi}{a}\right]^2 + \beta^2}} \quad (11)$$

$$U_{hn}^{L} = \frac{1}{j\omega\mu} \frac{j\beta E_{xn} + \left[\frac{n\pi}{a}\right] E_{zn}}{\sqrt{\left[\frac{n\pi}{a}\right]^2 + \beta^2}} \quad (12)$$

$$U_{en}^{L} = \frac{Y_{nL}^{TM}}{j\omega\epsilon} \frac{\left[\frac{n\pi}{a}\right] E_{xn} + j\beta E_{zn}}{\sqrt{\left[\frac{n\pi}{a}\right]^2 + \beta^2}} \quad (13)$$

where the field coefficients E_{xn} and E_{zn} are found from the amplitudes $\boldsymbol{X}$ and $\boldsymbol{Z}$ in (9) as

$$E_{xn} = \boldsymbol{P}_n^T \cdot \boldsymbol{X} \quad (14)$$

$$E_{zn} = \boldsymbol{P}_n^T \cdot \boldsymbol{Z}. \quad (15)$$

It is noted that the coefficients U_n are found to be purely real for all finline modes by virtue of the fact that the coefficients $j\beta E_{zn}$ are always real; also the coefficients E_{xn}

are always real. Since the fundamental finline mode is essentially TE in the slot, the coefficients E_{zn} can often be neglected altogether.

With detailed knowledge of the finline fields, we are now in a position to evaluate power flow, slot voltage, wall currents, losses, etc. Furthermore, having obtained the fields in the form of (5), integrals with x have been reduced to simple summations.

III. Obstacle Formulation

As an alternative to the aperture formulation and in order to effect a comparison, an obstacle-type solution based on an expansion for the fin currents was also investigated.

Using the concept of a transverse equivalent network, a set of integral equations defining a relationship between electric fields in the gap and the fin currents can be readily obtained as

$$\begin{bmatrix} -E_x^{\mathrm{L}} \\ \frac{a}{\pi}\frac{\partial}{\partial x}E_z^{\mathrm{L}} \end{bmatrix} = \begin{bmatrix} \tilde{Z}_{11}^{\mathrm{L}} & \tilde{Z}_{12}^{\mathrm{L}} \\ \tilde{Z}_{21}^{\mathrm{L}} & \tilde{Z}_{22}^{\mathrm{L}} \end{bmatrix} \begin{bmatrix} J_X \\ -\frac{\pi}{a}\int J_Z\,dx \end{bmatrix} \tag{16}$$

for fields infinitesimally left of $y = 0$ and as

$$\begin{bmatrix} E_x^{\mathrm{R}} \\ -\frac{a}{\pi}\frac{\partial}{\partial x}E_z^{\mathrm{R}} \end{bmatrix} = \begin{bmatrix} \tilde{Z}_{11}^{\mathrm{R}} & \tilde{Z}_{12}^{\mathrm{R}} \\ \tilde{Z}_{21}^{\mathrm{R}} & \tilde{Z}_{22}^{\mathrm{R}} \end{bmatrix} \begin{bmatrix} J_X \\ -\frac{\pi}{a}\int J_Z\,dx \end{bmatrix} \tag{17}$$

for fields to the right.

Hence by adding (1) and (2), we obtain the integral equation for resonance:

$$\begin{bmatrix} \tilde{Z}_{11} & \tilde{Z}_{12} \\ \tilde{Z}_{21} & \tilde{Z}_{22} \end{bmatrix} \begin{bmatrix} J_X \\ -\frac{\pi}{a}\int J_Z\,dx \end{bmatrix} = 0 \tag{18}$$

with $\tilde{Z}_{11} = \tilde{Z}_{11}^{\mathrm{L}} + \tilde{Z}_{11}^{\mathrm{R}}$, etc. This formulation, therefore, is based upon a common fin current distribution to both sides of the resonance equation, i.e., an assumption of continuous currents in the equivalent circuit.

In order to employ an appropriate set of basis functions, it is convenient to slightly redefine the axis positioning to that of Fig. 3. Green's impedance operators may be obtained using orthogonality as before. Moreover, symmetry about $x = a/2$ implies that only the functions $\phi_{hn}(x)$ corresponding to n even are involved in these operators.

In applying the Galerkin method, (16) and (17) are expanded directly onto a set of functions defined over the fin and including the appropriate edge condition. Such an expansion is possible in terms of Gegenbauer polynomials chosen to be orthogonal under the weight function:

$$W(x) = \sqrt{1 - \left[\frac{x}{t}\right]^2}$$

which introduces the required edge condition at $x = +t$.

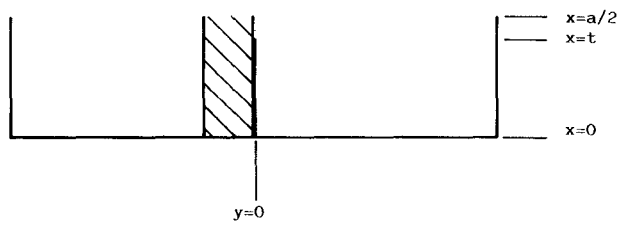

Fig. 3 Axis orientation for obstacle formulation.

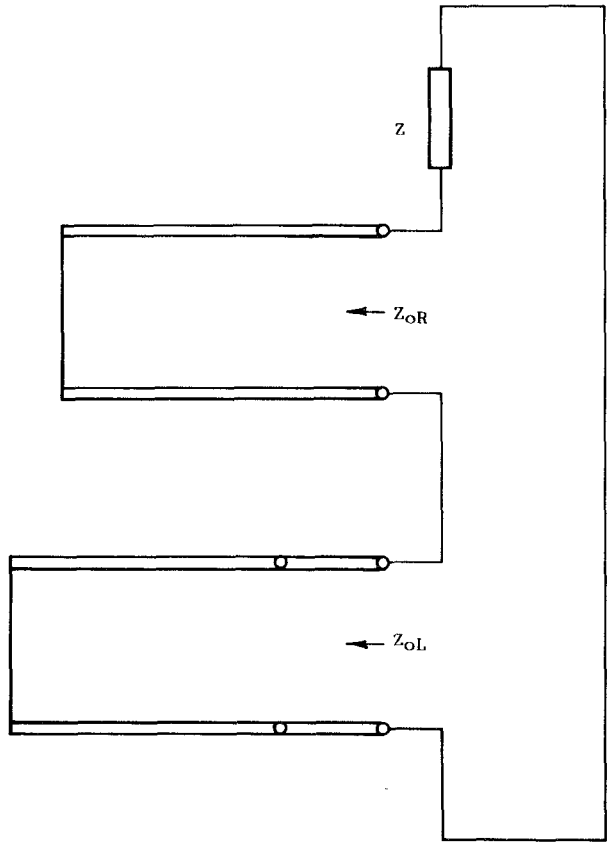

Fig. 4. Series equivalent circuit.

The current expansions may therefore be defined as

$$J_x(x) = \sum_{m=0}^{M} JX_m \sqrt{1-u^2}\, C_m^1(u) \tag{19}$$

$$\frac{\pi}{a}\int J_z(x) = \sum_{m=0}^{M} JZ_m \sqrt{1-u^2}\, C_m^1(u) \tag{20}$$

where $u = x/t$ and $C_m^1(u)$ are the appropriate Gegenbauer polynomials of order m. These are only defined over the region $0 < x < t$ since the current densities $J_x(x)$ and $J_z(x)$ cannot exist in the aperture region. Thus the range of integration within the impedance operators is also restricted to this range.

With the help of the above basis, integral equation (18) is more conveniently written as a matrix equation:

$$\begin{bmatrix} \boldsymbol{Z}_{11} & \boldsymbol{Z}_{12} \\ \boldsymbol{Z}_{21} & \boldsymbol{Z}_{22} \end{bmatrix} \cdot \begin{bmatrix} \boldsymbol{JX} \\ -\boldsymbol{JZ} \end{bmatrix} = 0 \tag{21}$$

where $\boldsymbol{JX}$, for instance, is a column vector of the coeffi-

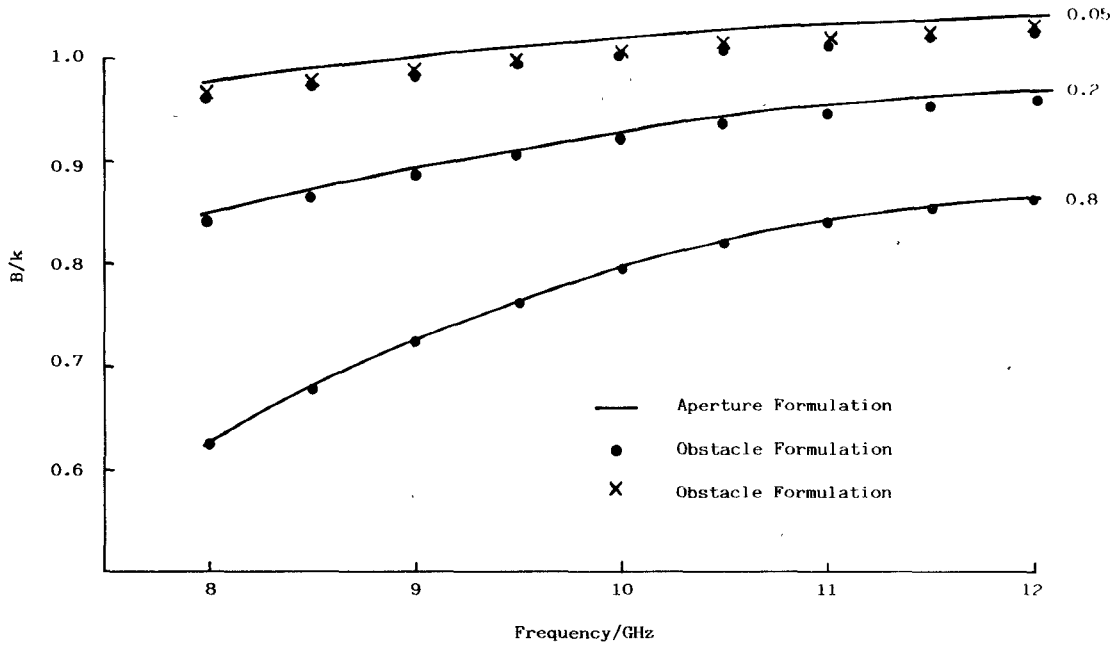

Fig. 5. Comparison of finline dispersion curves for various values of normalized fin gaps (w/a).

cients JX_m, and

$$\boldsymbol{Z}_{11}^{\mathrm{L}} = \sum_{n=0}^{\infty} Z_{11n}^{\mathrm{L}} \boldsymbol{Q}_n \cdot \boldsymbol{Q}_n^T.$$

The coefficients Q_{nm} are defined as

$$Q_{nm} = \int_0^t \sqrt{1-u^2}\, C_m^1(u)\, \phi_{hn}(tu)\, du.$$

The analytic evaluation of these coefficients is given in Appendix III.

It will be found that $n = 0$ components only arise again in $\boldsymbol{Z}_{11}$, and as with the aperture formulation, this fundamental component may be taken out of the matrix system, so that (21) becomes

$$Z_0 + Z_s = 0 \tag{22}$$

where $Z_0 = Z_{0\mathrm{R}}^{\mathrm{TE}} + Z_{0\mathrm{L}}^{\mathrm{TE}}$ and the series fin impedance z_s is given by

$$\frac{1}{z_s} = \boldsymbol{Q}_0^T \cdot \left[\boldsymbol{Z}_{11} - \boldsymbol{Z}_{12} \cdot \boldsymbol{Z}_{22}^{-1} \cdot \boldsymbol{Z}_{21}\right]^{-1} \cdot \boldsymbol{Q}_0.$$

This may therefore be interpreted as the resonance of the series equivalent circuit, as in Fig. 4. As the fins vanish into the side walls, the impedance z_s becomes large and solution approaches the impedance pole in Z_0 (defining modes in the dielectrically loaded waveguide and identical to the condition $Y_0 = 0$).

Numerical implementation of (22) was improved by making use of the quasi-static components to form impedance sums from which the frequency variation had been removed. These have to be evaluated numerically, whereas the Schwinger approach enabled such infinite sums to be evaluated analytically.

Results

Dispersion results for the fundamental mode over a range of fin gaps were found to be in close agreement with the aperture formulation, proving the validity of the obstacle approach. Samples of dispersion curves are presented in Fig. 5. However of more interest are the convergence properties of the Gegenbauer polynomial expansion for the fin currents.

It was found in general that matrix orders of at least 3 by 3 were required to achieve convergence in the J_x expansion, although the longitudinal current was essentially given by one term. This is shown in Table I, which gives the expansion coefficients obtained at 10 GHz for three different fin gaps.

While the two formulations are in close agreement, the aperture formulation yields marginally faster convergence of the expansion for the slot field, necessitating a lower matrix order. The applicability of Gegenbauer polynomials has been demonstrated and a satisfactory means of formulation established (despite the initial choice of divergent impedances). Thus, although finline is best solved in terms of an aperture formulation, the obstacle approach may be superior in other E-plane structures such as suspended strip line.

IV. Current Distributions

Using the theory described above, the wall currents for various finline modes were investigated. For the moment we shall consider the fundamental mode only.

The currents within a closed metallic waveguide fall into two categories: the circulating currents induced by H_z at the metallic surfaces and the axial currents induced by the transverse magnetic fields. In finline, the former currents rise from zero at the fin edge, divide at the intersection of

TABLE I
FIN CURRENTS EXPANSION COEFFICIENTS JX_m AND JZ_m FOR VARIOUS NORMALIZED FIN GAPS AT X-BAND

X-band finline, F = 10.0 Ghz, w/a = 0.050.		
	JX_m	JZ_m
1	-0.145653	1.000000
2	-0.037377	0.115555
3	-0.010047	0.007631
4	-0.004687	0.014367

X-band finline, F = 10.0 Ghz, w/a = 0.200.		
	JX_m	JZ_m
1	-0.055179	1.000000
2	-0.054885	0.143113
3	-0.003898	-0.015850
4	-0.005063	0.012464

X-band finline, F = 10.0 Ghz, w/a = 0.800.		
	JX_m	JZ_m
1	-0.520287	1.000000
2	-0.311005	0.496639
3	-0.194383	0.309794
4	-0.133317	0.215881

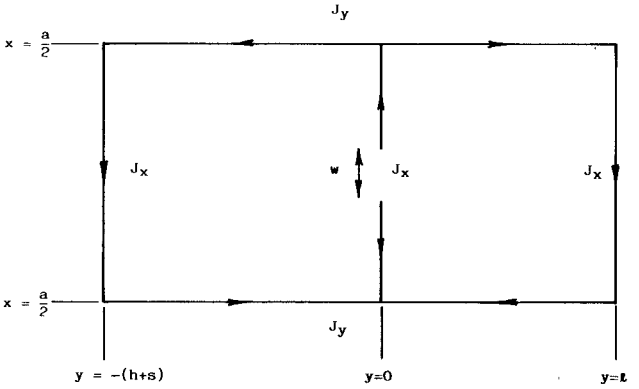

Fig. 6. Schematic diagram of finline circulating currents

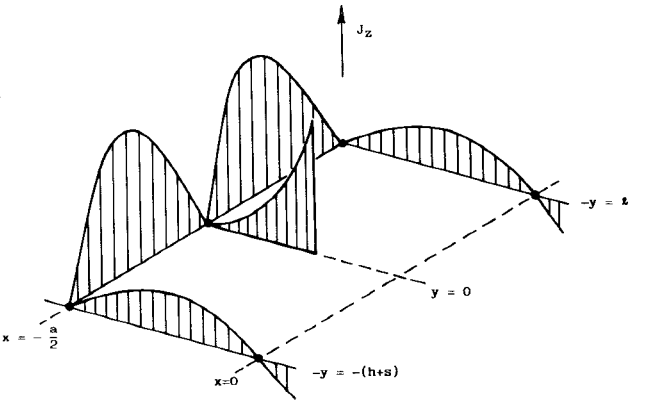

Fig 7. Schematic isometric diagram of axial currents.

the fins with the housing, and circulate around to the other fin edge, as illustrated in Fig. 6. For the fundamental mode, the distribution of these currents shows little variation around the guide apart from zeros of order $r^{0.5}$ at the fin edges. It is therefore apparent that the current node which is present in the broad wall of conventional waveguide operating in the fundamental TE_{01} mode is displaced onto the edges of the intruding fins. This is of major practical significance, since the construction technique commonly employed with conventional waveguides utilizes this node as the mating point between two machinings. This method, however, now is highly problematic when applied to finline because of the reason above and it requires in practice improved forms of choking, such as the one described in [9].

The axial currents are found from H_x and H_y depending on the direction of the normal. Here the wall currents are modified in the opposite sense, as shown in a schematic isometric form in Fig. 7. The central current maximum in the broad wall of the waveguide operating in the TE_{01} mode becomes split into two maxima, with a node appearing at the intersection of the fins and the housing where x- and y-directed magnetic field cannot exist. However, of more significance to the losses is the edge condition on the fins which gives rise to a singularity of $r^{-0.5}$ in the transverse fields. Although it may be argued that the edge effect is weakened by the fact that the skin depth is much less than the metallization thickness, there is evidence to suggest that at 10 GHz, where the skin depth in copper is approximately 1 μm, the singularity is still of the order of $r^{-0.5}$ for a metallization thickness of approximately 35 μm (1 oz/ft^2).

V. LOSS CALCULATIONS—COMPARISON WITH EXPERIMENT

The attentuation factor due to the conductor losses is obtained using the standard perturbational expression:

$$\alpha_c = \frac{R_s \int |H_t|^2 \, dl}{2 \iint \boldsymbol{E} \times \boldsymbol{H} \cdot a_z \, dS} \tag{23}$$

where R_s is the surface resistance given by $R_s = \omega\mu\rho/2$, where ρ is the resistivity.

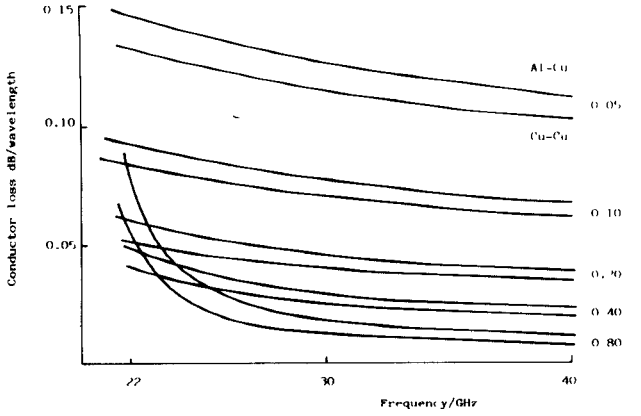

Fig. 8. Theoretical loss curves for various normalized fin gaps (w/a).

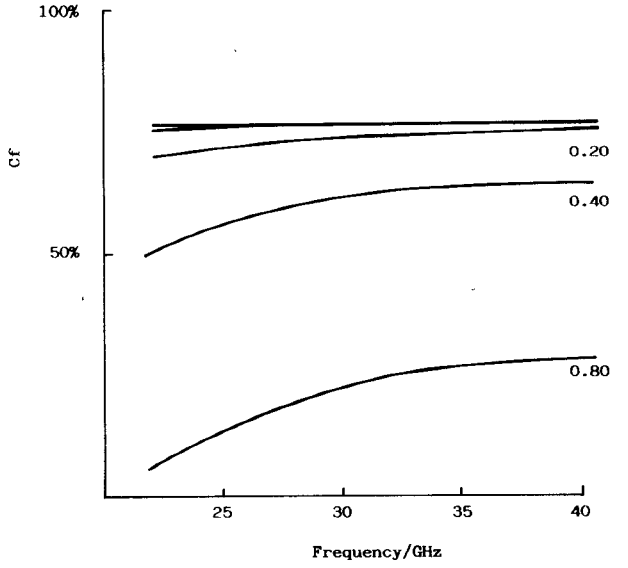

Fig. 9. Curves of Cf, the proportion of power dissipated on the fins for various normalized in fin gaps (w/a) copper housing and fins.

In performing the above calculations, it was possible to make a distinction between losses due to the fins and those due to the housing. Moreover the evaluation of the power flow integral allows one to quantify the proportion of power within the dielectric. From knowledge of the power flow, the "finline impedance" was derived using the definition

$$Z = \frac{V_s^2}{P} \tag{24}$$

where the quantity P is the power flow given by the denominator of (23) and V_s is the slot voltage obtained simply from the slot field E_x.

Fig. 8 shows calculated loss per wavelength in Q-band finline for various fin and housing metals, while Fig. 9 shows the proportion of power dissipated on the fins. As expected, this proportion increases rapidly as the fins intrude into the guide. However, reducing the normalized fin gap below 0.2, i.e., within the range of fin gaps found in practice, produces little further change.

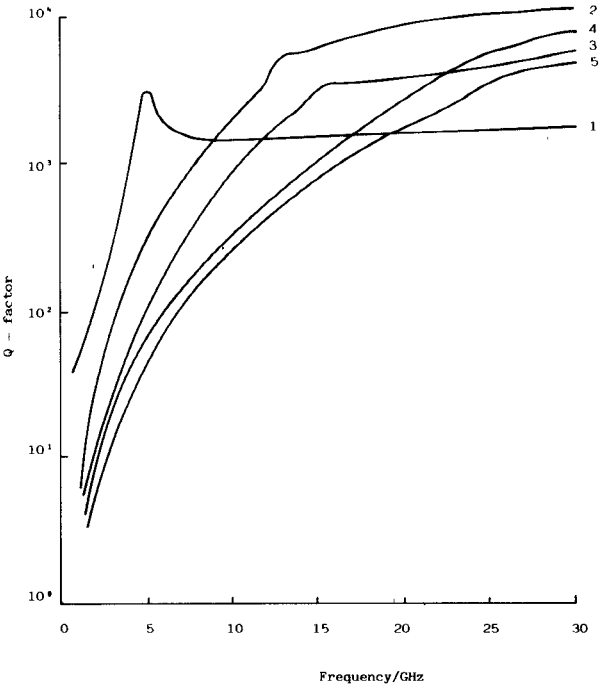

Fig. 10 Q Factors for the first five modes in X-band finline.

It is noted that slot fields are linked to the transverse model fields, whereas housing currents are predominantly due to the longitudinal magnetic fields and are consequently of a circulating nature.

A smaller fin gap will increasingly concentrate transverse fields to the slot region with increased fin currents, but in order to support these, the housing currents must also increase. This ultimately retains a fixed ratio between the two losses. The housing material therefore has an appreciable influence on the overall conduction losses, as those due to the singularity at the fin edges do not swamp all other losses.

In order to allow a comparison with experiment, the Q factor defined by

$$Q = \frac{2\pi \times \text{total energy stored per unit length}}{\text{total energy dissipated per unit length per cycle}} \tag{25}$$

was also calculated. This also provides a useful quantity when applied to (evanescent) higher order modes and for comparison between transmission media.

The total stored energy is obtained by evaluating

$$\overline{W} = \int \epsilon |E|^2 \, dS. \tag{26}$$

Fig. 10 presents results on calculated Q factor versus frequency for the first few finline modes, including the effect of dielectric losses for completeness. The cutoff points in the first three modes can be seen from the peaks indicated, although this effect seems to become less pronounced as mode order increases. Within the operating range of the fundamental mode, the higher order mode Q factors are increasingly rapidly from the collapse in value at low frequency. The second mode in particular has a very high Q factor, once propagating, due to its very small interaction with the fins.

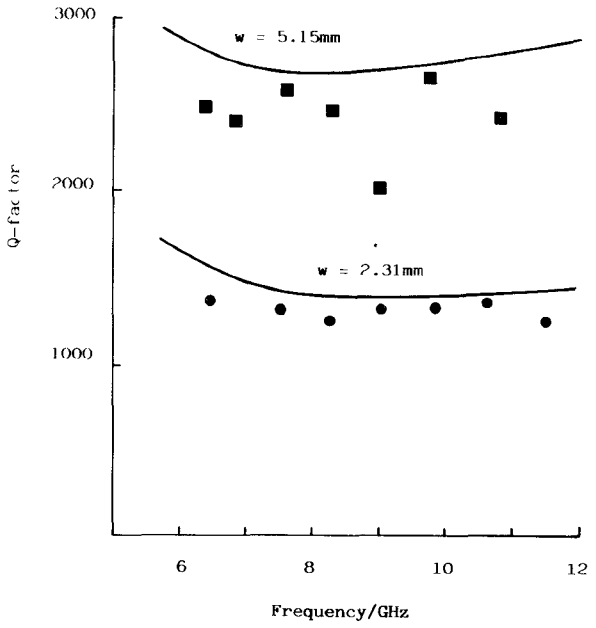

Fig. 11 Theoretical Q factors compared with experimental points for X-band finline.

Fig. 11 shows a comparison between calculated and measured Q factor in X-band finline. It can be seen that there is a very good agreement with theory for the narrower fin gap, giving a Q factor of the order of 1000. For the wider fin gap, where the Q factor is predicted to be of the order of 2500, miscellaneous losses therefore are seen to have a much greater impact. Although an improved form of choke virtually eliminated leakage along the structure, problems still remained, with the end shorts required to form the finline resonator producing the greater variance in results for the wider fin gap. However, even these results at least show finline losses to be of the order of those predicted.

VI. Conclusions

We have presented a rigorous calculation of currents and conduction losses in unilateral finline, comparing an aperture formulation to an obstacle formulation of the problem for the fundamental and higher order modes. The results indicate higher than hitherto predicted values of losses, in agreement with experiment.

Appendix I
Field Distributions

Here the functions $E_{xn}(y)$, $E_{yn}(y)$, etc., used in the construction of the spatial field variations are given.

A. $E_{xn}(y)$

Region (1): $-(h+s) < y < -s$:

$$E_{xn}(y) = \frac{n\pi}{a}\frac{\coth(k_n^s s+\theta_{en})}{k_n^s}\frac{\frac{n\pi}{a}E_{xn}+j\beta E_{zn}}{k_n^2} \cdot \frac{\epsilon_r\cosh\theta_{en}}{\cosh k_n^a h}\frac{k_n^a\sinh k_n^a(y+h+s)}{\cosh(k_n^s s+\theta_{en})} + \omega\mu\beta\frac{j\beta E_{xn}+\frac{n\pi}{a}E_{zn}}{j\omega\mu k_n^2}\frac{\sinh\theta_{hn}}{\sinh k_n^a h} \cdot \frac{\sinh k_n^a(y+h+s)}{\sinh(k_n^s s+\theta_{hn})}. \quad \text{(A1)}$$

Region (2): $-s < y < 0$:

$$E_{xn}(y) = \frac{n\pi}{a}\frac{\coth(k_n^s s+\theta_{en})}{k_n^s}\frac{\frac{n\pi}{a}E_{xn}+j\beta E_{zn}}{k_n^2} \cdot \frac{k_n^s\sinh[k_n^s(y+s)+\theta_{en}]}{\cosh(k_n^s s+\theta_{en})} + \omega\mu\beta\frac{j\beta E_{xn}+\frac{n\pi}{a}E_{zn}}{j\omega\mu k_n^2}\frac{\sinh[k_n^s(y+s)+\theta_{hn}]}{\sinh(k_n^s s+\theta_{hn})}. \quad \text{(A2)}$$

Region (3): $0 < y < \iota$:

$$E_{xn}(y) = E_{xn}\frac{\sinh k_n^a(\iota-y)}{\sinh k_n^a \iota}. \quad \text{(A3)}$$

B. $E_{zn}(y)$

Region (1): $-(h+s) < y < -s$:

$$E_{zn}(y) = -j\beta\frac{\coth(k_n^s s+\theta_{en})}{k_n^s}\frac{\frac{n\pi}{a}E_{xn}+j\beta E_{zn}}{k_n^2}\frac{\epsilon_r\cosh\theta_{en}}{\cosh k_n^a h} \cdot \frac{k_n^a\sinh k_n^a(y+h+s)}{\cosh(k_n^s s+\theta_{en})} + j\omega\mu\frac{n\pi}{a}\frac{j\beta E_{xn}+\frac{n\pi}{a}E_{zn}}{j\omega\mu k_n^2}\frac{\sinh\theta_{hn}}{\sinh k_n^a h} \cdot \frac{\sinh k_n^a(y+h+s)}{\sinh(k_n^s s+\theta_{hn})}. \quad \text{(A4)}$$

Region (2): $-s < y < 0$:

$$E_{zn}(y) = -j\beta\frac{\coth(k_n^s s+\theta_{en})}{k_n^s}\frac{\frac{n\pi}{a}E_{xn}+j\beta E_{zn}}{k_n^2} \cdot \frac{k_n^s\sinh[k_n^s(y+s)+\theta_{en}]}{\cosh(k_n^s s+\theta_{en})} + j\omega\mu\frac{n\pi}{a}\frac{j\beta E_{xn}+\frac{n\pi}{a}E_{zn}}{j\omega\mu k_n^2} \cdot \frac{\sinh[k_n^s(y+s)+\theta_{hn}]}{\sinh(k_n^s s+\theta_{hn})}. \quad \text{(A5)}$$

Region (3): $0 < y < \iota$:

$$E_{zn}(y) = E_{zn}\frac{\sinh k_n^a(\iota-y)}{\sinh k_n^a \iota}. \quad \text{(A6)}$$

C. $E_{yn}(y)$

Region (1): $-(h+s) < y < -s$:

$$E_{yn}(y) = \frac{\coth(k_n^s s + \theta_{en})}{k_n^s}\left[\frac{n\pi}{a}E_{xn} + j\beta E_{zn}\right] \cdot \frac{\epsilon_r \cosh\theta_{en}}{\cosh k_n^a h}\frac{\cosh k_n^a(y+h+s)}{\cosh(k_n^s s+\theta_{en})}. \quad \text{(A7)}$$

Region (2): $-s < y < 0$:

$$E_{yn}(y) = \frac{\coth(k_n^s s + \theta_{en})}{k_n^s}\left[\frac{n\pi}{a}E_{xn} + j\beta E_{zn}\right] \cdot \frac{\cosh[k_n^s(y+s)+\theta_{en}]}{\sinh(k_n^s s+\theta_{en})}. \quad \text{(A8)}$$

Region (3): $0 < y < \iota$:

$$E_{yn}(y) = -\frac{\coth k_n^a \iota}{k_n^a}\left[\frac{n\pi}{a}E_{xn} + j\beta E_{zn}\right]\frac{\cosh k_n^a(\iota - y)}{\cosh k_n^a \iota}. \quad \text{(A9)}$$

The magnetic fields are now given.

D. $H_{xn}(y)$

Region (1): $-(h+s) < y < -s$:

$$H_{xn}(y) = -\omega\epsilon\beta\frac{\coth(k_n^s s+\theta_{en})}{k_n^s}\frac{\frac{n\pi}{a}E_{xn} + j\beta E_{zn}}{k_n^2} \cdot \frac{\epsilon_r\cosh\theta_{en}}{\cosh k_n^a h}\frac{\cosh k_n^a(y+h+s)}{\cosh(k_n^s+\theta_{en})} - \frac{n\pi}{a}\frac{j\beta E_{xn} + \frac{n\pi}{a}E_{zn}}{j\omega\mu k_n^2}\frac{\sinh\theta_{hn}}{\sinh k_n^a h} \cdot \frac{k_n^a\cosh k_n^a(y+h+s)}{\sinh(k_n^s s+\theta_{hn})}. \quad \text{(A10)}$$

Region (2): $-s < y < 0$:

$$H_{xn}(y) = -\omega\epsilon\beta\frac{\coth(k_n^s s+\theta_{en})}{k_n^s}\frac{\frac{n\pi}{a}E_{xn} + j\beta E_{zn}}{k_n^2} \cdot \frac{\cosh[k_n^s(y+s)+\theta_{en}]}{\cosh(k_n^s s+\theta_{en})} - j\beta\frac{j\beta E_{xn} + \frac{n\pi}{a}E_{zn}}{j\omega\mu k_n^2} \cdot \frac{k_n^a\cosh[k_n(y+s)+\theta_{hn}]}{\sinh(k_n^s s+\theta_{hn})}. \quad \text{(A11)}$$

Region (3): $0 < y < \iota$:

$$H_{xn}(y) = j\omega\epsilon\frac{n\pi}{a}\frac{\coth k_n^a\iota}{k_n^a}\frac{\frac{n\pi}{a}E_{xn} - j\beta E_{zn}}{k_n^2} \cdot \frac{-\cosh k_n^a(\iota - y)}{\cosh k_n^a\iota} - \frac{n\pi}{a}\frac{j\beta E_{xn} + \frac{n\pi}{a}E_{zn}}{j\omega\mu k_n^2}\frac{-k_n^2\cosh k_n^s(\iota - y)}{\cosh k_n^a\iota}. \quad \text{(A12)}$$

E. $H_{zn}(y)$

Region (1): $-(h+s) < y < -s$:

$$H_{zn}(y) = j\omega\epsilon\frac{\coth(k_n^s s+\theta_{en})}{k_n^s}\frac{\frac{n\pi}{a}E_{xn} + j\beta E_{zn}}{k_n^2} \cdot \frac{\epsilon_r\cosh\theta_{en}}{\cosh k_n^a h}\frac{\cosh k_n^a(y+h+s)}{\cosh(k_n^s s+\theta_{en})} + j\beta\frac{j\beta E_{xn} + \frac{n\pi}{a}E_{zn}}{j\omega\mu k_n^2}\frac{\sinh\theta_{hn}}{\sinh k_n^a h} \cdot \frac{k_n^a\sinh k_n^a(y+h+s)}{\sinh(k_n^s s+\theta_{hn})}. \quad \text{(A13)}$$

Region (2): $-s < y < 0$:

$$H_{zn}(y) = j\omega\epsilon\frac{\coth(k_n^s s+\theta_{en})}{k_n^s}\frac{\frac{n\pi}{a}E_{xn} - j\beta E_{zn}}{k_n^2} \cdot \frac{\sinh[k_n^s(y+s)+\theta_{en}]}{\cosh(k_n^s s+\theta_{en})} + j\beta\frac{j\beta E_{xn} + \frac{n\pi}{a}E_{zn}}{j\omega\mu k_n^2} \cdot \frac{k_n^s\sinh[k_n^s(y+s)+\theta_{hn}]}{\sinh(k_n^s s+\theta_{hn})}. \quad \text{(A14)}$$

Region (3): $0 < y < \iota$:

$$H_{xn}(y) = j\omega\epsilon\frac{n\pi}{a}\frac{\coth k_n^a\iota}{k_n^a}\frac{\frac{n\pi}{a}E_{xn} - j\beta E_{zn}}{k_n^2} \cdot \frac{-\cosh k_n^a(\iota - y)}{\cosh k_n^a\iota} - \beta\frac{-j\beta E_{xn} + \frac{n\pi}{a}E_{zn}}{j\omega\mu k_n^2} \cdot \frac{-k_n^a\cosh k_n^s(\iota - y)}{\sinh k_n^a\iota}. \quad \text{(A15)}$$

F. $H_{yn}(y)$

Region (1): $-(h+s) < y < -s$:

$$H_{yn}(y) = \frac{1}{j\omega\mu}\left[j\beta E_{xn} + \frac{n\pi}{a}E_{zn}\right] \cdot \frac{\sinh\theta_{hn}}{\sinh k_n^a h}\frac{\sinh k_n^a(y+h+s)}{\sinh(k_{ns}^s+\theta_{hn})}. \quad \text{(A16)}$$

Region (2): $-s < y < 0$:

$$H_{yn}(y) = \frac{1}{j\omega\mu}\left[j\beta E_{xn}\frac{n\pi}{a}E_{zn}\right] \cdot \frac{\sinh\left[k_n^s(y+s)+\theta_{hn}\right]}{\sinh(k_n^s s+\theta_{hn})}. \quad \text{(A17)}$$

Region (3): $0 < y < \iota$:

$$H_{yn}(y) = \frac{1}{j\omega\mu}\left[-j\beta E_{xn} + \frac{n\pi}{a}E_{zn}\right]\frac{\sinh k_n^a(\iota - y)}{\sinh k_n^a \iota} \quad \text{(A18)}$$

where

$$k_n^a = \left[\frac{n\pi}{a}\right]^2 + \beta^2 - k_0^2$$

$$k_n^s = \left[\frac{n\pi}{a}\right]^2 + \beta^2 - \epsilon_r k_0^2$$

$$k_n = \left[\frac{n\pi}{a}\right]^2 + \beta^2.$$

Appendix II
Green's Admittances

The matrices appearing in (9) are obtained from the general expression

$$\boldsymbol{Y}_{ij} = \sum_n^{\infty} Y_{ijn}\boldsymbol{P}_n \cdot \boldsymbol{P}_n^T \quad \text{(A19)}$$

$$i = 1,2 \qquad j = 1,2$$

where

$$Y_{11n} = \left(Y_{n\mathrm{R}}^{\mathrm{TM}} + Y_{n\mathrm{L}}^{\mathrm{TM}}\right)\cos^2\tau_n + \left(Y_{n\mathrm{R}}^{\mathrm{TE}} + Y_{n\mathrm{L}}^{\mathrm{TE}}\right)\sin^2\tau_n$$

$$Y_{22n} = \frac{1}{n^2}\left(Y_{n\mathrm{R}}^{\mathrm{TE}} + Y_{n\mathrm{L}}^{\mathrm{TE}}\right)\cos^2\tau_n + \frac{1}{n^2}\left(Y_{n\mathrm{R}}^{\mathrm{TM}} + Y_{n\mathrm{L}}^{\mathrm{TM}}\right)\sin^2\tau_n$$

and

$$Y_{12n} = j\frac{1}{n}\sin^2\tau_n\cos^2\tau_n\left(Y_{n\mathrm{L}}^{\mathrm{TM}} - Y_{n\mathrm{R}}^{\mathrm{TM}} + Y_{n\mathrm{R}}^{\mathrm{TE}} - Y_{n\mathrm{L}}^{\mathrm{TE}}\right)$$

$$Y_{21n} = -Y_{12n}.$$

The summation starts from $n = 0$ only for the Y_{11} submatrix. All others start from $n = 1$, since E_z cannot have a fundamental component.

Appendix III

The coefficients Q_{nm} are obtained analytically from the result given in [10] so that

$$Q_{nm} = \frac{(-1)^m\pi\Gamma(2m+2)}{2m^1}\frac{J_{2m+1}(n\alpha)}{2n\alpha}\frac{\delta n}{a} \quad \text{(A20)}$$

where $\alpha = 2\pi t/a$. The relationship between the factorial and the gamma function of integer arguments allows further simplification, but first the small argument limit of the Bessel functions must be examined so as to determine the coefficients for the $n = 0$ case.

Consider the quotient appearing in (A20):

$$\frac{J_{2m+1}(n\alpha)}{2n\alpha}. \quad \text{(A21)}$$

Employing the small argument limit for the Bessel function gives

$$\frac{\left[\frac{n\alpha}{2}\right]^{2m+1}}{2n\alpha}\frac{1}{\Gamma(m+1)} = \frac{\left[\frac{n\alpha}{2}\right]^{2m}}{4\Gamma(m+1)}. \quad \text{(A22)}$$

It can be seen from the above that for $n = 0$, $Q_{nm} = 0$, unless $m = 0$, in which case

$$Q_{00} = \frac{1}{4}\frac{\pi}{a}. \quad \text{(A23)}$$

For $n > 0$, (A19) simplifies to

$$Q_{nm} = (-1)^m\pi(2m+2)\frac{J_{2m+1}(n\alpha)}{2n\alpha}\frac{2}{a} \quad \text{(A24)}$$

while for $n \to \alpha$ the asymptotic form is

$$Q_{nm} = (-1)^m\pi(2m+2)\frac{4}{an\pi\alpha}\frac{\cos\left[n\alpha - \frac{1-2m}{8m+4}\pi\right]}{2n\alpha}. \quad \text{(A25)}$$

From the above it can be seen that convergence of the coefficients Q_{nm} is very fast, and since they are known analytically, the integral equations may be readily converted into matrix form.

Acknowledgment

The authors wish to express their thanks to their colleagues P. Sargeaunt, C. Rycroft, and S. Clarke of GEC-Marconi Research Centre, Great Baddow, Chelmsford, Essex, for their support of this work.

References

[1] P. J. Meier, "Integrated fin-line millimeter components," *IEEE Trans. Microwave Theory Tech.*, vol. MTT-22, pp. 1200–1216, Dec. 1974.

[2] L.- P. Schmidt and T. Itoh, "Spectral domain analysis of dominant and higher order modes in fin-lines," *IEEE Trans. Microwave Theory Tech* , vol. MTT-28, pp. 981–985, Nov. 1980.

[3] J B Knorr and P M. Shayda, "Millimeter-wave fin-line characteristics," *IEEE Trans. Microwave Theory Tech.*, vol. MTT-28, pp. 737–743, July 1980

[4] A. S. Omar and K Schűnemann, "Formulation of the singular integral equation technique for planar transmission lines," *IEEE Trans Microwave Theory Tech.*, vol. MTT-33, pp. 1313–1321, Dec. 1985.

[5] R. Vahldieck, "Accurate hybrid-mode analysis of various finline configurations including multilayered dielectrics, finite metallization thickness, and substrate holding grooves," *IEEE Trans. Microwave Theory Tech.*, vol. MTT-32, pp. 1454–1460, Nov. 1984

[6] D Mirshekar-Syahkal and J B. Davies, "An accurate unified solution to various fin-line structures of phase constant characteristic impedance and attenuation," *IEEE Trans. Microwave Theory Tech* , vol. MTT-30, pp. 1854–1861, Nov. 1982.

[7] C. A. Olley and T. Rozzi, "Systematic characterization of the spectrum of unilateral finline," *IEEE Trans. Microwave Theory Tech.*, vol. MTT-34, pp. 1147–1156, Nov. 1986.
[8] R. E. Collin, *Field Theory of Guided Waves*. New York: McGraw-Hill, 1960.
[9] K. Tomiyasu and J. J. Bolus, "Characteristics of a new serrated choke," *IRE Trans. Microwave Theory Tech.*, vol. MTT-4, pp. 33–36, Jan. 1956.
[10] I. S. Gradshteyn and T. M. Ryzhik, *Tables of Integrals Series and Products*. New York: Academic Press, 1965, p. 830.

✠

Chris Olley was born in Bath, England, in 1960. He obtained the B.Sc (Hon) degree in 1983, and the Ph.D degree in electrical engineering from the University of Bath in June 1987. His research topic was the characterisation of finline and the work was sponsored by the Science and Engineering Research Council and GEC-Marconi Research at Great Baddow, Essex, where Dr. Olley is currently a member of staff.

Dr. Olley is a member of the Institution of Electrical Engineers (IEE) and of the Institution of Electronic and Radio Engineers (IERE), UK. He was awarded the IEE Student Prize in 1981 and the IEE South Western Region Young Members Award in 1985.

✠

T. Rozzi (M'66–SM'74) obtained the degree of 'Dottore' in physics from the University of Pisa in 1965 and the Ph.D. degree in electronic engineering at Leeds University in 1968. In June 1987 he received the degree of D.Sc from the University of Bath.

From 1968 to 1978 he was a Research Scientist at the Philips Research Laboratories, Eindhoven, the Netherlands, having spent one year, 1975, at the Antenna Laboratory, University of Illinois, Urbana. In 1975 he was awarded the Microwave Prize of the Microwave Theory and Technique Group of the Institute of Electrical and Electronic Engineers. In 1978 he was appointed to the Chair of Electrical Engineering at the University of Liverpool and subsequently was appointed to the Chair of Electronics and Head of the Electronics Group at the University of Bath in 1981. From 1983 to 1986 he held the additional responsibility of Head of the School of Electrical Engineering at Bath. Since 1986 Dr. Rozzi has also held the 'ordinary chair' of Antennas at the Faculty of Engineering, University of Ancona, Italy.